

# Pion electro-production in the Roper region in chiral quark models

B. Golli<sup>1</sup>, S. Širca<sup>2</sup>, and M. Fiolhais<sup>3</sup>

<sup>1</sup> Faculty of Education, University of Ljubljana and J. Stefan Institute, 1000 Ljubljana, Slovenia

<sup>2</sup> Faculty of Mathematics and Physics, University of Ljubljana and J. Stefan Institute, 1000 Ljubljana, Slovenia

<sup>3</sup> Department of Physics and Centre for Computational Physics, University of Coimbra, 3004-516 Coimbra, Portugal

November 2, 2018

**Abstract.** We present a method to calculate pion electro-production amplitudes in a coupled-channel framework incorporating quasi-bound quark-model states. The method offers a clear prescription how to extract the resonant part of the amplitudes, even in the presence of different decay channels and a strong mixing of neighbouring resonances. The method is applied to the calculation of the  $M_{1-}$  and the  $S_{1-}$  amplitudes in the P11 partial wave in a simple chiral quark model. A good agreement with the observed  $M_{1-}$  amplitude is found with a significant contribution from the pion cloud. The same effect is also prominent in the  $S_{1-}$  amplitude but a rather uncertain data prevent us to draw a definitive conclusion.

**PACS.** 11.80.Gw, 12.39.Ba, 13.60.Le, 14.20.Gk

## 1 Introduction

The study of baryon resonances above the inelastic threshold is frequently characterized by a strong interplay of different decay channels, mixing of different model states with equal quantum numbers, as well as the presence of background processes. These effects can almost completely obscure the relevant information about the resonance under investigation and make it hard to establish a clear connection of the data extracted in meson scattering and electro-weak processes to the properties obtained in model calculations. While these effects influence only little the properties of the lowest resonance  $\Delta(1232)$ , they are strongly present already in the case of the  $N(1440)$  (Roper) resonance.

In our previous work [1] we have developed a general method to incorporate excited baryons represented as quasi-bound quark-model states into a coupled channel calculation of pion scattering using the  $K$ -matrix approach. The method ensures unitarity through the symmetry of the  $K$  matrix as well as the proper asymptotic conditions. We were able to explain a rather intriguing behaviour of the scattering amplitudes in the region of the Roper resonance through the inclusion of the  $\pi\Delta$  and  $\sigma N$  inelastic channels. In this work we extend the formalism to the calculation of electro-production amplitudes.

The electromagnetic properties of the Roper resonance have been studied in several models involving quark, mesonic and/or gluonic degrees of freedom focusing mainly on the calculation of the electro-excitation part of the process. The constituent quark model, assuming a  $(1s)^2(2s)^1$  configuration, does not yield sensible results, even predict-

ing the wrong sign of the  $A_{1/2}$  amplitude at the photon point. It has been suggested that additional degrees of freedom, such as explicit excitations of the gluon field [2], the glueball field [3,4], or chiral fields [5] may be relevant for the formation of the Roper resonance. The importance of a correct relativistic treatment in constituent quark models has been emphasized in [6–10] yielding the correct sign at the photon point along with the sign change of  $A_{1/2}$  at  $Q^2 \sim 0.5$   $(\text{GeV}/c)^2$ . In order to reproduce its relatively large value at the photon point, the effects of the meson cloud have to be included as indicated in [11–13]. The quark charge densities inducing the nucleon to Roper transition have been determined from the phenomenological analysis [14] confirming the existence of a narrow central region and a broad outer band.

The present work is – to the best of our knowledge – the first attempt to apply a quark model of baryons to calculate full electro-production amplitudes in the case of a strong background and in the presence of open inelastic channels. Such processes are usually calculated in models based on baryon and meson degrees of freedom which involve numerous adjustable parameters, and in which resonances are incorporated in distinct ways. In the effective-Lagrangian unitary isobar model MAID [15] the electromagnetic resonant vertices are dressed (i.e. they already contain the meson-cloud contributions) while in the dynamical models, for example, DMT [16] or SL [17], the resonances are bare and the meson-cloud effects are generated dynamically. The dynamical models were put to thorough scrutiny when faced with a large body of data coming from recent  $N \rightarrow \Delta$  experiments, but only preliminary results exist in the Roper region [18].

In the next section we briefly review the construction of meson-baryon channel states which incorporate the quasi-bound quark-model states corresponding to the nucleon and its higher resonances. The construction of the multi-channel  $K$  matrix is discussed and the method to solve the Lippmann-Schwinger equation for the meson amplitudes is outlined.

In sec. 3 we give the formulas for the matrix elements of the multi-channel  $K$  matrix involving the photon-baryon channel, and the relation to the pion electro-production amplitude is established.

In sec. 4 we discuss the form of the production amplitude close to a resonance and explain how the resonant part of the amplitude can be isolated. Furthermore, we discuss the origin of different terms contributing to the background part of the amplitude.

The multipole expansion for the P11 wave is introduced in sec. 5 and the extraction of the helicity amplitudes from the corresponding electro-production amplitude is explained in sec. 6. We show that our method yields the standard relation between these two amplitudes and determines the relative sign between them.

We calculate the electro-production amplitudes in the region of the Roper resonance using the Cloudy Bag Model with the same set of parameters as used in the calculation of scattering amplitudes in our previous work. The results are presented and discussed in sec. 7 and summarized in the last section.

## 2 Incorporating quark-model states into a multi-channel formalism

We consider a class of chiral quark models in which mesons couple linearly to the quark core:

$$H' = \int dk \sum_{lmt} \left\{ \omega_k a_{lmt}^\dagger(k) a_{lmt}(k) + \left[ V_{lmt}(k) a_{lmt}(k) + V_{lmt}^\dagger(k) a_{lmt}^\dagger(k) \right] \right\}, \quad (1)$$

where  $a_{lmt}^\dagger(k)$  is the creation operator for a meson with angular momentum  $l$  and the third components of spin  $m$  and isospin  $t$ . If we include only  $l = 1$  pions, the form of the source is

$$V_{mt}^\pi(k) = -v(k) \sum_{i=1}^3 \sigma_m^i \tau_t^i. \quad (2)$$

The quark operator  $V_{lmt}(k)$  depends on the model and includes the possibility that the quarks change their radial function which is specified by the reduced matrix elements  $V_{BB'}(k) = \langle B || V(k) || B' \rangle$ , where  $B$  are the bare baryon states (e.g. the bare nucleon,  $\Delta$ , Roper, ...)

We have shown that in such models it is possible to find an exact expression for the  $K$  matrix without explicitly specifying the form of the asymptotic states. In the basis with good total angular momentum  $J$  and isospin  $I$ , the

elements of the  $K$  matrix take the form

$$K_{MB M'B'}^{JI} = -\pi \mathcal{N}_{MB} \langle \Psi_{JI}^{M'B'} || V^M(k) || \tilde{\Psi}_B \rangle, \quad \mathcal{N}_{MB} = \sqrt{\frac{\omega_M E_B}{k_M W}}, \quad E_B(k) = \sqrt{M_B^2 + k^2}, \quad (3)$$

where  $\omega_M$  and  $k_M$  are the energy and momentum of the meson. Here  $\Psi_{JI}^{M'B'}$  is the principal-value state corresponding to the channel specified by the meson  $M$  ( $\pi$ ,  $\sigma$ , ...) and the baryon  $B$  ( $N$ ,  $\Delta$ , ...):

$$|\Psi_{JI}^{MB}\rangle = \mathcal{N}_{MB} \left\{ \sum_{\mathcal{R}} c_{\mathcal{R}}^{MB} |\Phi_{\mathcal{R}}\rangle + [a^\dagger(k_M) \tilde{\Psi}_B]^{JI} + \sum_{M'B'} \int \frac{dk \chi_{JI}^{M'B' MB}(k)}{\omega_k + E_{B'}(k) - W} [a^\dagger(k) \tilde{\Psi}_{B'}]^{JI} \right\}, \quad (4)$$

normalized as

$$\langle \Psi_{J'I'}^{M'B'}(W') | \Psi_{JI}^{MB}(W) \rangle = \delta_{J'J} \delta_{I'I} (\delta_{M'B', MB} + \mathbf{K}_{M'B' MB}^2) \times \delta(W - W'). \quad (5)$$

where  $W$  is the invariant energy of the system. The first term is the sum over *bare* three-quark states  $\Phi_{\mathcal{R}}$  involving different excitations of the quark core, the next term, which defines the channel, corresponds to the free meson and the baryon, and the third term represents meson clouds around different isobars. The sum in the latter term includes also inelastic channels in which case the integration over the mass of the unstable intermediate hadrons ( $\sigma$ -meson,  $\Delta$ , ...) is implied. The state  $\tilde{\Psi}_B$  in (3) and (4) represents either the nucleon or the intermediate isobar decaying into the nucleon and the pion. In the latter case the state is described by (4) with  $MB = \pi N$  and normalized to  $\delta_{J'J} \delta_{I'I} \delta_{M'B', MB} \delta(M_B - M_B')$  (instead of (5)), where  $W$  has been replaced by the invariant mass of the  $\pi N$  system  $M_B$ . The on-shell meson amplitudes  $\chi_{JI}^{M'B' MB}$  are proportional to the corresponding matrix elements of the on-shell  $K$  matrix

$$K_{M'B' MB} = \pi \mathcal{N}_{M'B'} \mathcal{N}_{MB} \chi_{JI}^{M'B' MB}(k_{M'}). \quad (6)$$

From the variational principle for the  $K$  matrix it is possible to derive a set of integral equations for the  $\chi$  amplitude which is equivalent to the Lippmann-Schwinger equation for the  $K$  matrix. The resulting expression for  $\chi$  can be written in the form

$$\chi_{JI}^{M'B' MB}(k) = - \sum_{\mathcal{R}} \tilde{c}_{\mathcal{R}}^{MB} \tilde{\mathcal{V}}_{B'\mathcal{R}}^{M'}(k) + \mathcal{D}_{JI}^{M'B' MB}(k). \quad (7)$$

The states  $\Phi_{\mathcal{R}}$  are not eigenstates of the Hamiltonian and therefore mix:  $\tilde{\Phi}_{\mathcal{R}} = \sum_{\mathcal{R}'} u_{\mathcal{R}\mathcal{R}'} \Phi_{\mathcal{R}'}$ . As a consequence,

$$\tilde{\mathcal{V}}_{B\mathcal{R}}^M = \sum_{\mathcal{R}'} u_{\mathcal{R}\mathcal{R}'} \mathcal{V}_{B'\mathcal{R}'}^M, \quad \tilde{c}_{\mathcal{R}}^{MB} = \frac{\tilde{\mathcal{V}}_{B\mathcal{R}}^M}{Z_{\mathcal{R}}(W)(W - M_{\mathcal{R}})}, \quad (8)$$

where  $\mathcal{V}_{B\mathcal{R}}^M$  are the dressed matrix elements of the quark-meson interaction between the resonant state and the baryon state in channel  $MB$ , and  $Z_{\mathcal{R}}$  is the wave-function normalization.

### 3 The $\pi N$ electro-production amplitudes

The EM interaction Hamiltonian is assumed to be of the form

$$H_\gamma = \frac{1}{\sqrt{2\pi^3}} \int d\mathbf{k}_\gamma \sum_\mu \left[ \tilde{V}_\mu^\gamma(\mathbf{k}_\gamma) a_\mu(\mathbf{k}_\gamma) + \text{h.c.} \right],$$

where  $\mathbf{k}_\gamma$  and  $\mu$  are the momentum and the polarization of the incident photon, and

$$\tilde{V}_\mu^\gamma(\mathbf{k}_\gamma) = \frac{e_0}{\sqrt{2\omega_\gamma}} \int d\mathbf{r} \boldsymbol{\varepsilon}_\mu \cdot \mathbf{j}(\mathbf{r}) e^{i\mathbf{k}_\gamma \cdot \mathbf{r}}. \quad (9)$$

The state representing the photon-nucleon system reads

$$|\Psi_N(m_s, m_t; \mathbf{k}_\gamma, \mu)\rangle = \mathcal{N}_\gamma a_\mu^\dagger(\mathbf{k}_\gamma) |\Psi_N(m_s m_t)\rangle, \quad (10)$$

$$\mathcal{N}_\gamma = \sqrt{k_\gamma \omega_\gamma} \sqrt{\frac{E_N^\gamma}{W}}. \quad (11)$$

Here  $m_s$  and  $m_t$  are the third components of the nucleon spin and isospin,  $\omega_\gamma = (W^2 - M_N^2 - Q^2)/2W$ ,  $k_\gamma^2 = \omega_\gamma^2 + Q^2$ ,  $E_N^\gamma = W - \omega_\gamma$ , with  $Q^2$  measuring the photon virtuality. In the type of models we are considering here, the current and the charge density operators can be split into quark and pion parts:

$$\mathbf{j}(\mathbf{r}) = \bar{\psi} \boldsymbol{\gamma} \left( \frac{1}{6} + \frac{1}{2} \tau_0 \right) \psi + i \sum_t t \pi_t(\mathbf{r}) \nabla \pi_{-t}(\mathbf{r}), \quad (12)$$

$$\rho(\mathbf{r}) = \bar{\psi} \gamma_0 \left( \frac{1}{6} + \frac{1}{2} \tau_0 \right) \psi - i \sum_t t \pi_t(\mathbf{r}) P_{-t}^\pi(\mathbf{r}), \quad (13)$$

where  $P^\pi$  stands for the canonically conjugate pion field. The amplitude for pion electro-production on the nucleon is defined as

$$\mathcal{M}_{\pi N}^{JI} = -\frac{\mathcal{N}_\gamma}{\sqrt{k_0 k_\gamma}} \langle \Psi_{JI}^{(+)}(m_J m_I; k_0, l) | \tilde{V}_\mu^\gamma(\mathbf{k}_\gamma) | \Psi_N(m_s m_t) \rangle. \quad (14)$$

It is related to the corresponding  $T$  matrix through  $T = \sqrt{k_0 k_\gamma} / 8\pi \mathcal{M}$ . In (14)  $m_J$  and  $m_I$  are the third components of the spin and the isospin, and  $k_0$  is the outgoing pion momentum.

The  $K$ -matrix elements for electro-production corresponding to different channels  $MB$  ( $\pi N, \pi \Delta, \sigma N, \dots$ ) are introduced similarly as in (14) by replacing the state  $\Psi_{JI}^{(+)}$  by the principal-value state (14):

$$\mathcal{M}_{MB}^{KJI} = -\frac{\mathcal{N}_\gamma}{\sqrt{k_0 k_\gamma}} \langle \Psi_{JI}^{MB}(m_J m_I; k_0, l) | \tilde{V}_\mu^\gamma(\mathbf{k}_\gamma) | \Psi_N(m_s m_t) \rangle. \quad (15)$$

They are related to the electro-production amplitudes through  $\mathcal{M} = \mathcal{M}^K + iT\mathcal{M}^K$ . (This trivially follows from the Heitler's equation  $T = K + iTK$  since the proportionality factor between  $T$  and  $\mathcal{M}$  is the same as between  $K$  and  $\mathcal{M}^K$ .) In principle, the equation for  $\mathcal{M}$  involves also the matrix elements corresponding to Compton scattering, but they can be neglected since they are orders of

magnitude smaller than those containing the strong interaction. In the region of the Roper resonance in the P11 partial wave it suffices to consider only the  $\pi \Delta$  and the  $\sigma N$  inelastic channels and the equation reads

$$\begin{aligned} \mathcal{M}_{\pi N}(W) = & \mathcal{M}_{\pi N}^K(W) + i \left[ T_{\pi N \pi N}(W) \mathcal{M}_{\pi N}^K(W) \right. \\ & + \int_{M_N + m_\pi}^{W - m_\pi} dM_\Delta T_{\pi N \pi \Delta}(W, M_\Delta) \mathcal{M}_{\pi \Delta}^K(W, M_\Delta) \\ & \left. + \int_{2m_\pi}^{W - M_N} d\mu T_{\pi N \sigma N}(W, \mu) \mathcal{M}_{\sigma N}^K(W, \mu) \right]. \quad (16) \end{aligned}$$

Here  $M_\Delta$  denotes the invariant mass of the  $\pi N$  system originating from the decaying  $\Delta$  isobar and  $\mu$  the invariant mass of the two-pion system from the decaying  $\sigma$ -meson.

### 4 The behaviour of the amplitudes close to a resonance

From (6), (7) and (8) it follows that close to a resonance, denoted by  $\mathcal{R}$ , the  $K$ -matrix element between the elastic channel and an arbitrary channel  $MB$  can be split in the resonant and the background parts

$$K_{\pi N MB} = -\pi \sqrt{\frac{\omega_0 \omega_M E_N E_B}{k_0 k_M W^2}} \tilde{\mathcal{C}}_{\mathcal{R}}^{MB} \tilde{\Psi}_{N\mathcal{R}}^\pi(k_0) + K_{\pi N MB}^{\text{bkg}}. \quad (17)$$

Collecting the terms containing the coefficient  $\tilde{\mathcal{C}}_{\mathcal{R}}^{MB}$  in (4) and in (7) and expressing it in terms of  $K_{\pi N MB} - K_{\pi N MB}^{\text{bkg}}$  using (17), the principal-value state (4) takes the form

$$|\Psi_{JI}^{MB}\rangle = -K_{\pi N MB} \sqrt{\frac{k_0 W}{\pi^2 \omega_0 E_N}} \frac{\sqrt{\mathcal{Z}_{\mathcal{R}}}}{\tilde{\mathcal{V}}_{N\mathcal{R}}^\pi} |\widehat{\Psi}^{\text{res}}\rangle + |\Psi_{JI}^{MB(\text{bkg})}\rangle, \quad (18)$$

where

$$\begin{aligned} |\widehat{\Psi}^{\text{res}}\rangle = & \frac{1}{\sqrt{\mathcal{Z}_{\mathcal{R}}}} \left\{ |\Phi_{\mathcal{R}}\rangle - \int dk \frac{\tilde{\mathcal{V}}_{N\mathcal{R}}^\pi(k) [a^\dagger(k) |\Psi_N\rangle]^{JI}}{\omega_k + E_N(k) - W} \right. \\ & \left. - \sum_{MB} \int dk \frac{\tilde{\mathcal{V}}_{B\mathcal{R}}^M(k) [a^\dagger(k) |\widehat{\Psi}_B\rangle]^{JI}}{\omega_k + E_B(k) - W} \right\}, \quad (19) \end{aligned}$$

while  $\Psi_{JI}^{MB(\text{bkg})}$  has the form of (4) without the terms containing  $\tilde{\mathcal{C}}_{\mathcal{R}}^{MB}$  plus a term in the form of the resonant part of (18) in which  $K_{\pi N MB}$  is replaced by  $K_{\pi N MB}^{\text{bkg}}$ .

We can now split also the amplitude (15) into the resonant and the background parts:

$$\begin{aligned} \mathcal{M}_{MB}^K = & \sqrt{\frac{\omega_\gamma E_N^\gamma}{\pi^2 \omega_0 E_N}} \frac{\sqrt{\mathcal{Z}_{\mathcal{R}}}}{\mathcal{V}_{N\mathcal{R}}} K_{\pi N MB} \langle \widehat{\Psi}_{\mathcal{R}}^{\text{res}}(W) | \tilde{V}^\gamma | \Psi_N \rangle \\ & + \mathcal{M}_{MB}^{K(\text{bkg})}. \quad (20) \end{aligned}$$

We see that the resonant part depends on the channel indices only through the corresponding element of the scattering  $K$  matrix. Next we plug (20) into (16) and take into

account the relation between the  $T$  and the  $K$  matrices for scattering ( $T = K + iTK$ ). The resonant part of the electro-production amplitudes then reads

$$\mathcal{M}_{\pi N}^{(\text{res})} = -\sqrt{\frac{\omega_\gamma E_N^\gamma}{\pi^2 \omega_0 E_N}} \frac{\sqrt{Z_{\mathcal{R}}}}{\mathcal{V}_{N\mathcal{R}}} \langle \widehat{\Psi}_{\mathcal{R}}^{(\text{res})}(W) | \tilde{V}^\gamma | \Psi_N \rangle T_{\pi N \pi N}, \quad (21)$$

while the background part satisfies

$$\mathcal{M}_{\pi N}^{(\text{bkg})} = \mathcal{M}_{\pi N}^{K(\text{bkg})} + i \left[ T_{\pi N \pi N} \mathcal{M}_{\pi N}^{K(\text{bkg})} + \bar{T}_{\pi N \pi \Delta} \bar{\mathcal{M}}_{\pi \Delta}^{K(\text{bkg})} + \bar{T}_{\pi N \sigma N} \bar{\mathcal{M}}_{\sigma N}^{K(\text{bkg})} \right], \quad (22)$$

where  $\bar{T}$  and  $\bar{\mathcal{M}}$  are the amplitudes averaged over the invariant masses of the intermediate hadron using the averaging procedure introduced in [1]. The background part of (20) can be cast in the form

$$\mathcal{M}_{MB}^{K(\text{bkg})} = \sqrt{\frac{\omega_\gamma E_N^\gamma}{\omega_0 E_N}} \frac{K_{\pi N MB}^{(\text{bkg})}}{\pi \mathcal{V}_{N\mathcal{R}}^\pi(k_0)} \langle \widehat{\Psi}_{\mathcal{R}}^{(\text{res})} | \tilde{V}^\gamma | \Psi_N \rangle \quad (23)$$

$$+ \sqrt{\frac{\omega_\gamma \omega_M E_N^\gamma E_B}{k_0 k_M W^2}} \left[ \sum_{\mathcal{R}' \neq \mathcal{R}} c_{\mathcal{R}'}^{MB} \langle \widehat{\Psi}_{\mathcal{R}'} | \tilde{V}^\gamma | \Psi_N \rangle \right. \quad (24)$$

$$+ \langle \widehat{\Psi}_{\mathcal{R}}^{MB(\text{non})} | \tilde{V}^\gamma | \Psi_N \rangle \quad (25)$$

$$\left. + [\langle \Psi_B | a(k_M) ]^{JI} \tilde{V}^\gamma | \Psi_N \rangle \right]. \quad (26)$$

Here  $\widehat{\Psi}_{\mathcal{R}'}$  corresponds to a resonance  $\mathcal{R}'$  other than the chosen one (i.e.  $\mathcal{R}$ ) and has the form (19) with  $\mathcal{R}$  replaced by  $\mathcal{R}'$ ; the corresponding matrix element does not depend on the channel indices  $MB$ . In the P11 partial wave this type of contribution is dominated by the ground state in which case  $\Phi_{\mathcal{R}'}$  is replaced by the exact ground state  $\Psi_N$ . The state  $\widehat{\Psi}_{\mathcal{R}}^{MB(\text{non})}$  in (25) originates from the non-resonant part of (7); it has the form of (19) without the leading  $\Phi_{\mathcal{R}}$  and with  $\mathcal{D}_{JI}^{M'B' MB}(k)$  replacing  $\mathcal{V}_{N\mathcal{R}}$ . The last term (26) can be further manipulated by commuting  $a(k_0)$  through  $\tilde{V}^\gamma$ . From (1) it follows  $a_{mt}(k) | \Psi_N \rangle = -V_{mt}^\dagger(k) (\omega_k + H - M_N)^{-1} | \Psi_N \rangle$ , which yields (for  $I = J$ )

$$\begin{aligned} & \langle \Psi_{J'=I} | a(k) \rangle_{m_j m_I}^{JI=J} \tilde{V}_{L\mu}^{T0} | \Psi_N m_s m_t \rangle = \\ & - \sum_j g_{\frac{1}{2} J' j}^{JLT} \frac{\langle \Psi_{J'} | \tilde{V}_L^T | \Psi_j \rangle \langle \Psi_N | V(k) | \Psi_j \rangle}{\omega_k + E_j(k) - M_N} C_{\frac{1}{2} m_s L \mu}^{J m_J} C_{\frac{1}{2} m_t T 0}^{J m_I} \\ & + \langle \Psi_{J'} m'_s m'_t | [a_{mt}(k), \tilde{V}_{L\mu}^{T0}] | \Psi_N m_s m_t \rangle C_{J' m'_s L \mu}^{J m_J} C_{J' m'_t T 0}^{J m_I}. \end{aligned} \quad (27)$$

Here  $\tilde{V}_{L\mu}^{T0}$  is a chosen multipole of the EM interaction (discussed in the next section) where  $T = 0$  and  $1$  stand for the isoscalar and the isovector part, respectively, and  $g_{J' j}^{JLT} = (2J'+1)(2J''+1)W(LJ'J''1; jJ)W(TJ'J''1; jJ)$ , where  $W$  are the Racah coefficients. The first term leads to a u-channel contribution with the intermediate states  $\Psi_j$  dominated by the nucleon and the delta, while the second term corresponds to the pion pole term.

## 5 Multipole decomposition

Expanding (9) into multipoles, we have for the  $M_{1-}$  and the  $S_{1-}$  amplitudes:

$$\begin{aligned} M_{1-}^{(1/2)} &= -\sqrt{\frac{\omega_\gamma E_N^\gamma}{6k_0 W}} \langle \Psi_{JI}^{(+)} | \tilde{V}_{(T=1)}^{M1} | \Psi_N \rangle, \\ M_{1-}^{(0)} &= -\sqrt{\frac{\omega_\gamma E_N^\gamma}{18k_0 W}} \langle \Psi_{JI}^{(+)} | \tilde{V}_{(T=0)}^{M1} | \Psi_N \rangle, \end{aligned} \quad (28)$$

$$\begin{aligned} S_{1-}^{(1/2)} &= -\sqrt{\frac{\omega_\gamma E_N^\gamma}{2k_0 W}} \langle \Psi_{JI}^{(+)} | \tilde{V}_{(T=1)}^{C0} | \Psi_N \rangle, \\ S_{1-}^{(0)} &= -\sqrt{\frac{\omega_\gamma E_N^\gamma}{6k_0 W}} \langle \Psi_{JI}^{(+)} | \tilde{V}_{(T=0)}^{C0} | \Psi_N \rangle, \end{aligned} \quad (29)$$

related to  $\pi^0$  production amplitude on the proton and neutron as

$${}_{p,n} M_{1-}^{(1/2)} = M_{1-}^{(0)} \pm \frac{1}{3} M_{1-}^{(1/2)}, \quad (30)$$

and analogously for the  $S_{1-}$ . Here

$$\tilde{V}^{C0}(k_\gamma) = \sqrt{\frac{4\pi\alpha}{2\omega_\gamma}} \int d\mathbf{r} \rho_{\text{EM}} j_0(k_\gamma r) \quad (31)$$

is the Coulomb multipole. The same formulas apply to the  $\mathcal{M}^K$  amplitudes that enter (21) and (22) provided  $\Psi_{JI}^{(+)}$  is replaced by (4).

## 6 Helicity amplitudes

At the resonant energy ( $W = M_{\mathcal{R}}$ ) the transition amplitude appearing in (21) between the ground state and the resonant state  $\widehat{\Psi}_{\mathcal{R}}^{\text{res}}$  corresponds to the helicity amplitude for electro-excitation of the resonance. While the sign of the electro-production amplitudes is fixed by (28) and (29), the sign of the helicity amplitude (as well as the sign of the pion decay amplitude) depends on the relative phase between the wave functions of the excited state and the ground state. The helicity amplitudes for the Roper resonance are defined [10], [15] as

$$A_{1/2} = -\xi_{\mathcal{R}} \langle \widehat{\Psi}_{\mathcal{R}}^{\text{res}}(m'_s = \frac{1}{2}) | \tilde{V}^{M1} | \Psi_N(m_s = -\frac{1}{2}) \rangle, \quad (32)$$

$$S_{1/2} = -\xi_{\mathcal{R}} \langle \widehat{\Psi}_{\mathcal{R}}^{\text{res}}(m'_s = \frac{1}{2}) | \tilde{V}^{C0} | \Psi_N(m_s = \frac{1}{2}) \rangle. \quad (33)$$

Here  $\xi_{\mathcal{R}} = \text{sign}(g_{\pi N \mathcal{R}}/g_{\pi N N})$ . Since  $\omega_\gamma$  does not enter the final expression for the production amplitudes, it has been adopted to use the value  $\omega_\gamma(Q^2 = 0) \equiv k_W$  in the denominator of (9) and in the numerator of (28) and (29) also in the region  $Q^2 \neq 0$ .

We now show that our formalism yields the familiar relation between the electro-production and helicity amplitudes. From (21), (28) and (30) it follows

$$\text{Im } {}_p M_{1-}^{(1/2)} = -\frac{1}{3} \sqrt{\frac{k_W E_N^\gamma}{6\pi^2 \omega_0 E_N}} \frac{\sqrt{Z_{\mathcal{R}}}}{\mathcal{V}_{N\mathcal{R}}^\pi} \text{Im} T_{\pi N \pi N} \left( -\frac{3}{\sqrt{2}} \right) \times \langle \widehat{\Psi}_{\mathcal{R}}^{\text{(res)}} (m_s = \frac{1}{2}) | \tilde{V}^{M1} | \Psi_N (m_s = -\frac{1}{2}) \rangle,$$

where the factor  $(-3/\sqrt{2})$  comes from the Clebsch-Gordan coefficients relating the reduced matrix elements in (28) to the matrix element with the third components of spin and isospin ( $m_s, m'_s, m_t = m'_t = \frac{1}{2}$ ). The amplitude  $\mathcal{V}_{N\mathcal{R}}^\pi$  can be expressed in terms of the elastic width of the resonance

$$\Gamma_{\pi N} = 2\pi \frac{\omega_0 E_N \mathcal{V}_{N\mathcal{R}}^\pi(k_0)^2}{Z_{\mathcal{R}} k_0 W}. \quad (34)$$

Using  $\text{Im} T_{\pi N \pi N} = \Gamma_{\pi N} / \Gamma$  (at  $W = M_{\mathcal{R}}$ ) we obtain

$$\text{Im } {}_p M_{1-}^{(1/2)} = -\xi_{\mathcal{R}} \sqrt{\frac{k_W E_N^\gamma \Gamma_{\pi N}}{6\pi k_0 M_{\mathcal{R}} \Gamma^2}} A_{1/2}^p, \quad (35)$$

and similarly

$$\text{Im } {}_p S_{1-}^{(1/2)} = \xi_{\mathcal{R}} \sqrt{\frac{k_W E_N^\gamma \Gamma_{\pi N}}{3\pi k_0 M_{\mathcal{R}} \Gamma^2}} S_{1/2}^p. \quad (36)$$

The above expressions differ from the standard one by  $E_N^\gamma$  appearing instead of the nucleon rest mass  $M_N$ . This is a consequence of the normalization of our quark-model many-body state representing the recoiled nucleon which is normalized to 1 rather than to  $M_N/E_N$ . Adopting this convention requires us to slightly increase the  $g_{\pi NR}$  coupling constant ( $\sim 5\%$ ) in order to reproduce the results with the normalization to unity.

## 7 Results

We have performed the calculation of the electro-production amplitudes using the Cloudy Bag Model (CBM) with the same choice of parameters as in the calculation of the scattering amplitudes [1]. We use the same bag radius for the excited states as for the ground state. For  $v(k)$  appearing in (2) we have

$$v(k) = r_q \frac{1}{2f} \frac{k^2}{\sqrt{12\pi^2 \omega_k}} \frac{\omega_{\text{MIT}}^0}{\omega_{\text{MIT}}^0 - 1} \frac{j_1(kR)}{kR},$$

where  $r_q = 1$  if  $v(k)$  is evaluated between the states in the  $(1s)^3$  configuration,  $r_q = r_\omega$  for the transition between the  $(1s)^2(2s)^1$  and the  $(1s)^3$  configuration, and  $r_q = \frac{2}{3} + r_\omega^2$  between the  $(1s)^2(2s)^1$  configurations. Here

$$r_\omega = \frac{1}{\sqrt{3}} \left[ \frac{\omega_{\text{MIT}}^1 (\omega_{\text{MIT}}^0 - 1)}{\omega_{\text{MIT}}^0 (\omega_{\text{MIT}}^1 - 1)} \right]^{1/2}, \quad (37)$$

with  $\omega_{\text{MIT}}^0 = 2.043$  and  $\omega_{\text{MIT}}^1 = 5.396$ . We have adopted the conventional value of  $f = 76$  MeV which reproduces

the  $\pi NN$  coupling constant. The free parameters of the model are the bag radius  $R$  and the energies of the bare quark states corresponding to the nucleon and the excited states. The choice of the positive sign of (37) fixes the relative sign between the quark spinors in the  $1s$  and  $2s$  state and implies  $\xi_{\mathcal{R}} = +1$  in (32) and (33). In particular, we have for the upper components  $u_{2s}(R)/u_{1s}(R) > 0$ .

The vector mesons have not been included in our calculation of the scattering amplitudes since their contribution turns out to be almost negligible in the considered energy range. For electro-production, however, phenomenological approaches reveal a relatively important contribution of the  $\omega$ -meson already at lower energies. We have therefore included the phenomenological form of its contribution to the  $K$  matrix in the elastic channel in the form

$${}_p M_{1-}^{(1/2)}(\omega\text{-meson}) = \frac{1}{3} \frac{M_N}{4\pi W m_\pi} \frac{g_{\gamma\pi\omega} g_{\omega 1} k_\gamma k_\pi \rho_\omega(k_\omega)}{m_\omega^2 - m_\pi^2 + 2k_\gamma \omega_\pi},$$

where the corresponding form-factor is calculated in our model as (see e.g. [19])

$$\rho_\omega(|\mathbf{k}_\omega|) = \int dr r^2 j_0(|\mathbf{k}_\omega| r) (u(r)^2 + v(r)^2).$$

We use  $g_{\gamma\pi\omega} = 0.374\sqrt{4\pi/137}$  while the strong coupling is less known and is usually assumed to lie in the range  $8 < g_{\omega 1} < 20$ .

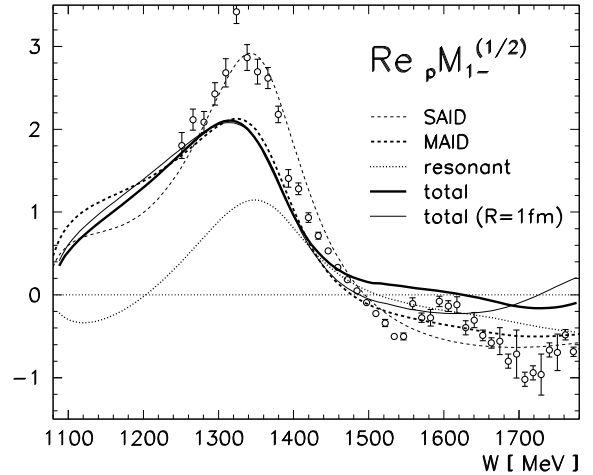


**Fig. 1.** The real part of the  ${}_p M_{1-}^{(1/2)}$  amplitude at  $Q^2 = 0$  for the P11 partial wave, calculated with  $R_{\text{bag}} = 0.83$  fm (solid thick line) and with  $R_{\text{bag}} = 1.00$  fm (thin line). The resonant contribution is shown separately. The experimental points are the single-energy solutions of the SAID partial-wave analysis [20]; the “SAID” curve shows the corresponding fit; the MAID result is from [15].

In figs. 1-4 we present the results for the  ${}_p M_{1-}^{(1/2)}$  and  ${}_n M_{1-}^{(1/2)}$  amplitudes. Using  $R = 0.83$  fm and keeping the same set of model parameters as determined in the scattering case we reproduce reasonably well the experimental amplitudes. The agreement improves if we include the contribution of the  $\omega$ -meson using  $g_{\omega 1} = 8$ . At energies below

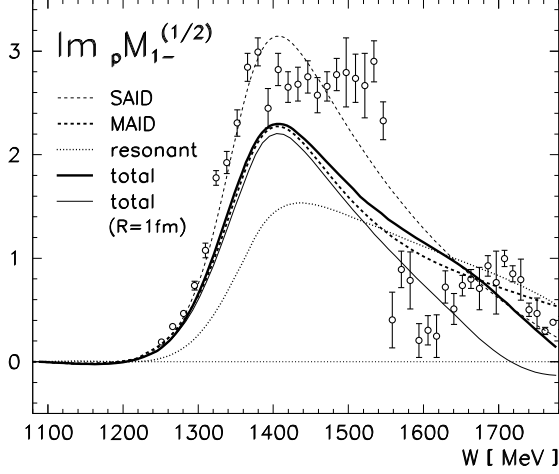


Fig. 2. The imaginary part of  ${}_p M_{1-}^{(1/2)}$ . Notation as in fig. 1.

the resonance the amplitudes are dominated by the background. This is in marked contrast to the P33 case in the region of the  $\Delta(1232)$  which have been extensively investigated in our previous works (see e.g. [21] and [22]). The photo-production amplitude in the case of the  $\Delta(1232)$  is dominated by the resonant contribution and follows the shape of the elastic  $T$  matrix in accordance with (21).

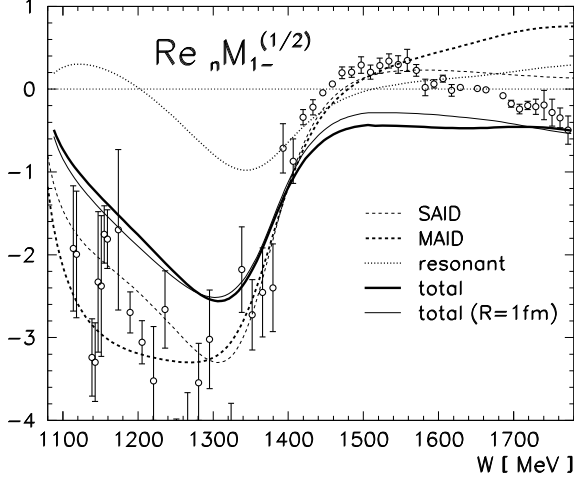


Fig. 3. The real part of  ${}_n M_{1-}^{(1/2)}$ . Notation as in fig. 1.

It is interesting to study different contributions to the total amplitude shown in figs. 5 and 6. At lower energies they are dominated by a huge negative contribution of the nucleon pole (24), the non-resonant term (25), the term (26) containing the u-channel isobar exchange (the first term of (27)) dominated by the  $\Delta(1232)$ , as well as the pion pole term (the second term in (27)). Above the two pion threshold, the  $\pi\Delta$  channel becomes important while the contribution from the  $\sigma N$  channel turns out to be insignificant.

Taking into account the limitations and the drawbacks of the CBM that reproduces the static properties of the

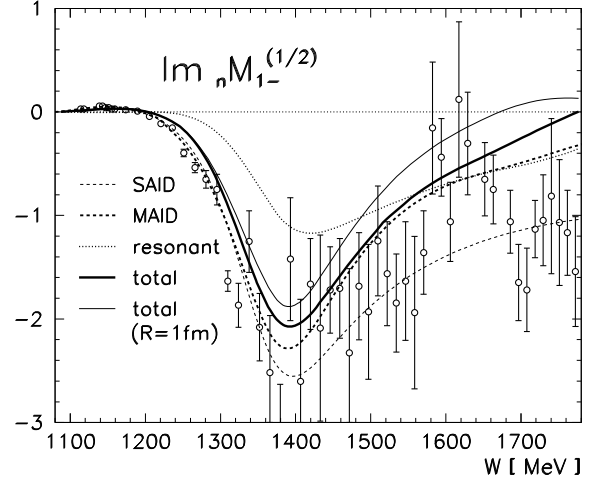


Fig. 4. The imaginary part of  ${}_n M_{1-}^{(1/2)}$ . Notation as in fig. 1.

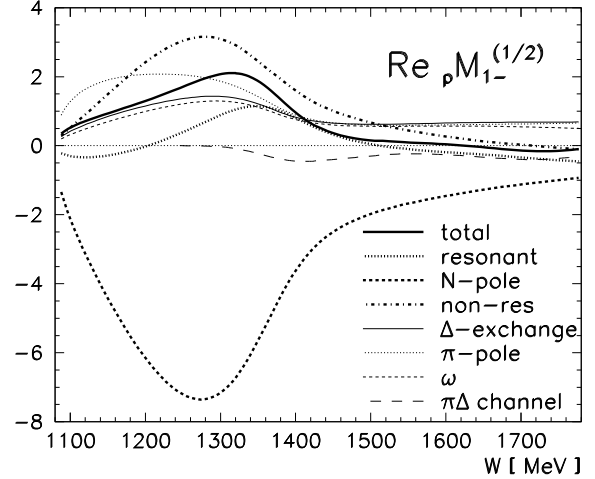


Fig. 5. Contributions to  $\text{Re}_p M_{1-}^{(1/2)}$  (see text).

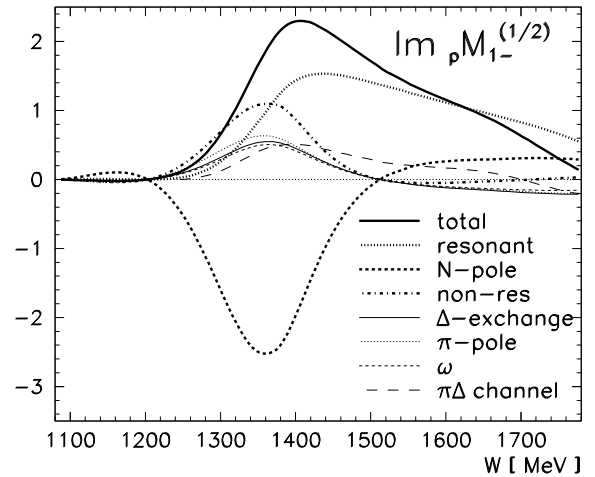
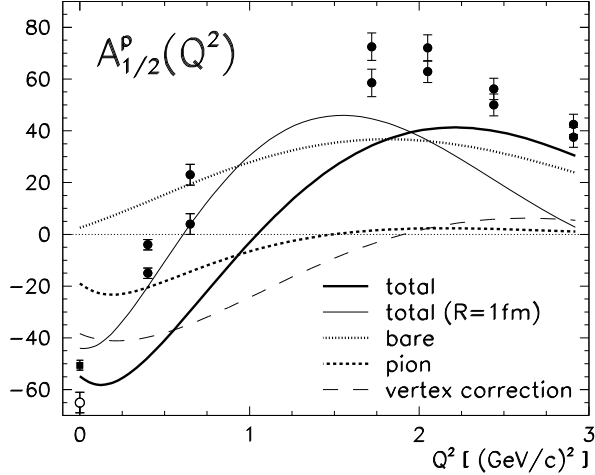


Fig. 6. Contributions to  $\text{Im}_p M_{1-}^{(1/2)}$  (see text).

nucleon only at the level of 10 % to 20 %, we have not considered the possibility to readjust the model parameters

in order to fit better the experiment. We can nonetheless conclude that the model successfully explains the main features of the  $M_{1-}$  amplitude. The sensitivity on the variation of the bag radius (see the thin solid line in figs. 1-4) is weak except at higher energies where our model anyway fails to reproduce the scattering amplitudes above  $R_{\text{bag}} \sim 1$  fm.

Regarding the transverse helicity amplitude for the proton displayed in fig. 7, we reproduce the value at the photon point in agreement with the calculation of [13] within the same quark model. This value is dominated by the pion cloud effects while the contribution from the bare quark core is almost negligible. At higher  $Q^2$  the quark core contribution becomes stronger and positive while that of the pions diminishes. As a result the amplitude exhibits a zero crossing which occurs at a somewhat higher  $Q^2$  than the one extracted from the experiment. This signifies that the pion cloud contribution may be overestimated. Taking a larger bag radius of  $R_{\text{bag}} \sim 1$  fm at which the strength of the pion cloud becomes weaker brings the zero-crossing value of  $Q^2$  in the ballpark of acceptable values. A similar behaviour of the core contribution and the pionic effects has been obtained in [12] using a completely different model for the quark-pion coupling. The recent calculation in the SL model [18] also indicates a strong meson cloud contribution.



**Fig. 7.** Helicity amplitude  $A_{1/2}^p(Q^2)$  at the pole of the  $K$  matrix ( $W = 1530$  MeV). The separate contributions include the  $3q$  core, the  $\gamma\pi\pi'$  interaction, and the pion-cloud corrections to the  $\gamma BB'$  vertex. Empty circle: PDG value [23]; full square and circles: analyses of newer JLab experiments. Two values at each  $Q^2 \neq 0$  correspond to two different extraction approaches (see [24] for details).

Such a conclusion cannot be drawn in the case of the scalar amplitude especially in the energy range of the resonance (and above), due to the rather uncertain experimental situation as well as the cancellation of different relatively large contributions to the calculated amplitude. Since the experimental values are not available except in the energy range of the resonance we compare

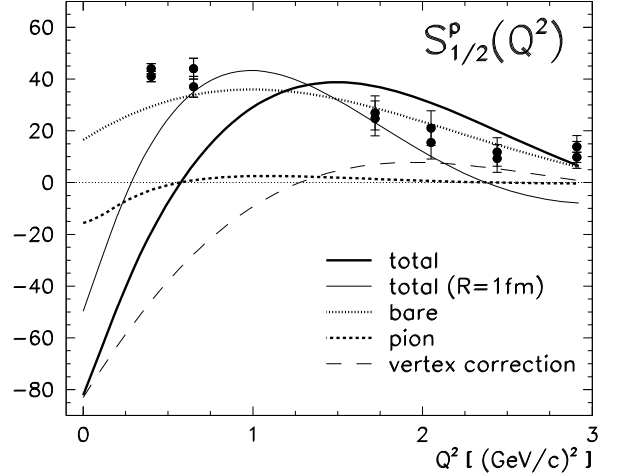


**Fig. 8.** Helicity amplitude  $S_{1/2}^p(Q^2)$ . Notation as in fig. 7.

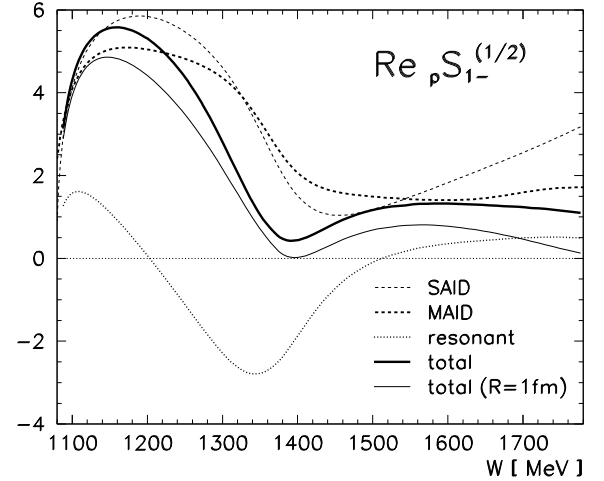


**Fig. 9.** The real part of  ${}_p S_{1-}^{(1/2)}$ . Notation as in fig. 1.

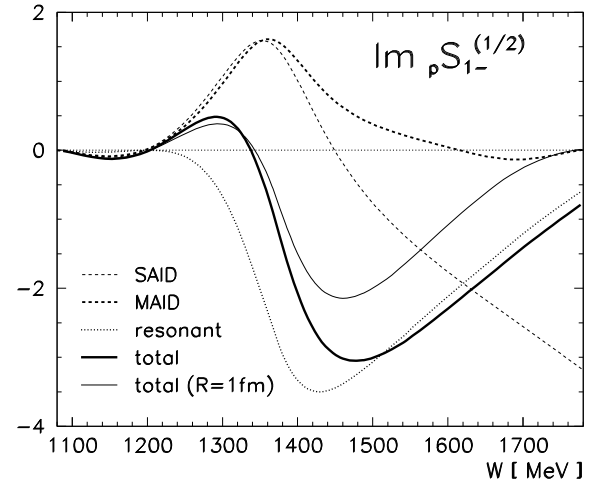


**Fig. 10.** The imaginary part of  ${}_p S_{1-}^{(1/2)}$ . Notation as in fig. 1.

our results to the values deduced from the MAID and SAID analysis for  ${}_p S_{1-}^{(1/2)}$  as shown in figs. 9 and 10. For

$Q^2 \rightarrow 0$ , a reasonably good agreement is obtained only below  $\sim 1300$  MeV; above, the imaginary part of our amplitude crosses zero much sooner than those of the phenomenological models and reaches a relatively large negative value at the resonant energy. This is due to the effects of the pion cloud which are large and have the opposite sign with respect to the contribution from the quark core which is small at  $Q^2 \rightarrow 0$ . In fact, this is the consequence of the same mechanism that governs the behaviour of the magnetic helicity amplitude which can be seen by comparing the helicity amplitude  $S_{1/2}$  in fig. 8 to  $A_{1/2}$  in fig. 7. A similar pattern for the two contributions has been found in [12] but with a substantially weaker pion cloud contribution which does not yield the zero crossing of  $S_{1/2}$ . Note that the phenomenological analysis from SAID also yields a negative value for the scalar pion production amplitude at  $Q^2 \rightarrow 0$  in the energy region of the resonance, while the values from MAID [15] remain small and positive.

## 8 Conclusions

Compared with the analysis of the scattering amplitudes in our previous work [1], the study of electro-production amplitudes offers further insight in the dynamics of the underlying quark model. Taking into account the approximate nature of the Cloudy Bag Model and the fact that we have not included any new free parameters (except for the strong  $\omega$  vertex), we have been able to reproduce surprisingly well the main features of the  $M_{1-}$  electro-production amplitude in the energy range from the threshold up to  $W \sim 1700$  MeV and for  $Q^2$  up to  $\sim 3$  GeV<sup>2</sup>/c<sup>2</sup>. Our investigation has pointed out the important – and in several cases the dominant – role played by the pion cloud, especially in the region of low  $Q^2$ , being gradually overwhelmed by the dynamics of the quark core as we go towards higher  $Q^2$ , supporting the picture in which the pion cloud dictates the long-range while the quark core the short-range physics of the baryon [25].

For the reasons discussed in the previous section we are not able to assess the quality of our prediction in the case of the scalar amplitude. Yet, our approach gives a rather definitive prediction for the behaviour of the  $S_{1/2}$  helicity amplitude for  $Q^2 \rightarrow 0$  which is expected to become small or even negative in this limit.

Though we have used a relatively simple model to obtain the results in a particular partial wave, the method is applicable to a broad class of models. Application of the method using more sophisticated models for the quark-meson dynamics could – when tested with more selective data coming from planned double-polarization experiments at MAMI and Jefferson Lab – finally lead to the solution of the Roper puzzle.

One of the authors (S. Š.) would like to express his thanks for helpful discussions with Inna Aznauryan and Lothar Tiator.

## References

1. B. Golli and S. Širca, Eur. Phys. J. A **38**, 271 (2008).
2. Zhenping Li, Volker Burkert, and Zhujun Li, Phys. Rev. D **46**, 70 (1992).
3. W. Broniowski, T. D. Cohen and M. K. Banerjee, Phys. Lett. B **187**, 229 (1987).
4. P. Alberto, M. Fiolhais, B. Golli, and J. Marques, Phys. Lett. B **523**, 273 (2001).
5. O. Krehl, C. Hanhart, S. Krewald, and J. Speth, Phys. Rev. C **62**, 025207 (2000).
6. S. Capstick, Phys. Rev. D **46**, 2864 (1992); S. Capstick and B. D. Keister, Phys. Rev. D **51**, 3598 (1995).
7. H. J. Weber, Phys. Rev. C **41**, 2783 (1990).
8. F. Cardarelli, E. Pace, G. Salmè and S. Simula, Phys. Lett. B **397**, 13 (1997).
9. B. Juliá-Díaz, D. O. Riska, F. Coester, Phys. Rev. C **69**, 035212 (2004).
10. I. G. Aznauryan, Phys. Rev. C **76**, 025212 (2007); I. G. Aznauryan et. al., arXiv: 0810.0997 [nucl-th].
11. F. Cano and P. González, Phys. Lett. B **431**, 270 (1998).
12. Y. B. Dong, K. Shimizu, A. Faessler, and A. J. Buchmann, Phys. Rev. C **60**, 035203 (1999).
13. K. Bermuth, D. Drechsel and L. Tiator, Phys. Rev. D **37**, 89 (1988).
14. L. Tiator, M. Vanderhaeghen, Phys. Lett. B **672**, 344 (2009).
15. D. Drechsel, S. S. Kamalov, L. Tiator, Eur. Phys. J. A **34**, 69 (2007).
16. S. S. Kamalov, S. N. Yang, D. Drechsel, O. Hanstein, L. Tiator, Phys. Rev. C **64** 032201 (2001).
17. A. Matsuyama, T. Sato, T.-S. H. Lee, Phys. Reports **439**, 193 (2007).
18. B. Juliá-Díaz, et al., arXiv:0904.1918 [nucl-th].
19. P. Alberto, S. S. Avancini, and M. Fiolhais, Int. Journal of Modern Phys. E **14**, 1171 (2005).
20. R. Arndt et al., Phys. Rev. C **52** (1995) 2120; R. Arndt et al., Phys. Rev. C **69**, 035213 (2004).
21. M. Fiolhais, B. Golli, S. Širca, Phys. Lett. B **373**, 229 (1996).
22. P. Alberto, L. Amoreira, M. Fiolhais, B. Golli, and S. Širca, Eur. Phys. J. A **26**, 99 (2005).
23. C. Amsler et al. (Particle Data Group), Phys. Lett. B **667**, 1 (2008).
24. I. G. Aznauryan et al. (CLAS Collaboration), Phys. Rev. C **71**, 015201 (2005); I. G. Aznauryan et al. (CLAS Collaboration), Phys. Rev. C **78**, 045209 (2008). The value at the photon point is from M. Dugger et al. (CLAS Collaboration), Phys. Rev. C **76**, 025211 (2007).
25. V. Burkert, AIP Conf. Proc. 1056, 348 (2008).